IEEE Photonics Journal
An IEEE Photonics Society Publication

Open Access

Hybrid Computational Near-Eye Light Field Display

Volume 11, Number 1, February 2019

Jian Zhao
Qungang Ma
Jun Xia
Jun Wu
Bintao Du
Hao Zhang

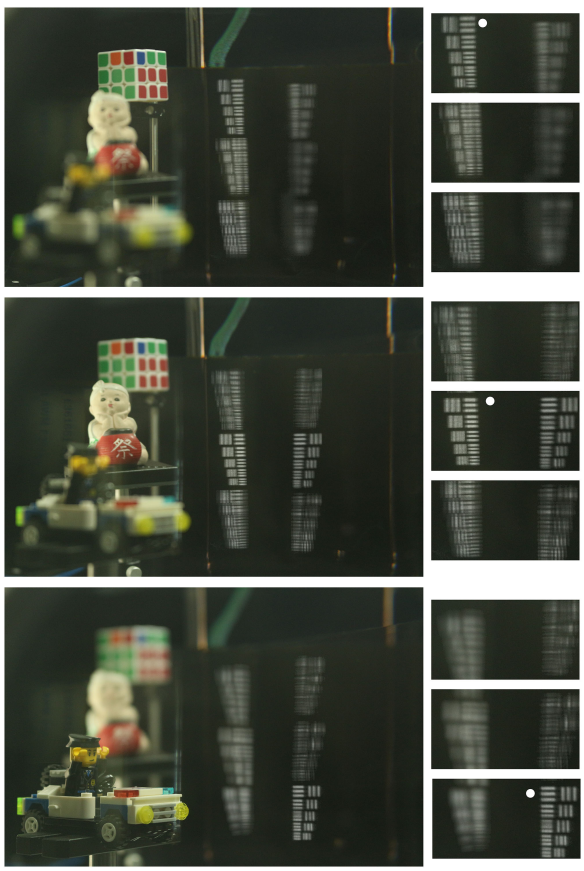

DOI: 10.1109/JPHOT.2019.2893934
1943-0655

IEEE photonics SOCIETY

IEEE

Hybrid Computational Near-Eye Light Field Display

Jian Zhao,[1] **Qungang Ma**,[2] **Jun Xia**,[1] **Jun Wu**,[1] **Bintao Du**,[1] **and Hao Zhang**[1]

[1]School of Electronic Science and Engineering, Southeast University, Nanjing 210096, China
[2]School of Electronic and Computer Engineering, Peking University, Shenzhen 518055, China

DOI:10.1109/JPHOT.2019.2893934

Manuscript received January 1, 2019; accepted January 15, 2019. Date of publication January 31, 2019; date of current version February 8, 2019. This work was supported by the National Key R&D Program of China (2017YFB1002900) and the Fundamental Research Funds for the Central Universities (KYLX15_0212). Corresponding authors: Jun Xia and Jun Wu (e-mail: xiajun@seu.edu.cn; wujunseu@seu.edu.cn).

Abstract: We propose a hybrid computational near-eye light field display based on microlens arrays (MLAs) and structure parameters prioritization method (SPPM) that can render correct accommodation and expand the depth of field (DOF). The proposed display consists of two MLAs and two micro-displays. Two sets of depth-sliced images are superimposed to reconstruct the object's light field. The system's ray resolution and the spectra difference between the proposed light field and the conventional one are discussed. The DOF of the proposed system is extended without the requiring of high refresh rate display. Furthermore, SPPM is proposed to extend the spatial frequency of the light field. A prototype is demonstrated and the experimental result shows that the depth field of the reconstructed images is significantly increased compared with conventional near-eye light field display based on single MLA.

Index Terms: Near eye display, augmented/virtual reality, light field display.

1. Introduction

Near-eye displays have attracted extensive attention over the past several decades. The Virtual Reality (VR) and Augmented Reality (AR) use the near-eye display to show the virtual object floating in front of the eye. People can perceive depth information from the virtual scene though the size perspective, the motion parallax, the overlap (or Interposition), the shading and the accommodation. In order to provide comfortable and high-resolution 3D virtual scene, it is crucial to reduce Accommodation-Convergence (AC) conflict problem due to the inaccurate focus cues, such as eye accommodation and retinal blur effects [1]–[3]. Eye accommodation refers that the eye can focus on a fixated object with a clarity of retinal image by changing the refractive power of the crystalline lens under the contraction and relaxation of the ciliary muscles. Moreover, the retinal image will appear blurry for the object which is far away from the eye's accommodative distance. The failure of rendering accurate focus cues leads to distorted depth perception and visual discomfort [4] in the conventional three-dimensional near-eye displays (3D-NED). Recently, several types of 3D-NED have been proposed to resolve the AC conflict problem and expand the DOF, including holographic displays, volumetric displays, multi-focal plane displays and light field displays.

However, there are still a lot of challenges among these methods. Holographic displays [5], [6] can reconstruct accurate wave front of real object via phase and amplitude modulation, but the system demands complex computation and bulky optical elements which against to the miniaturization for 3D-NED. Volumetric displays [4], [7] synthesize a virtual multifocal display using a fast switchable lens synchronized with a single display, but it has to be working under a high refresh rate. For the category of multi-focal plane displays, including additive [5], [8]–[10] and multiplicative display [11]–[16], the DOF of the virtual object is severely limited by the gaps between the adjacent display units. Note that, large DOF and the powerful modulation of light rays can effectively suppress the AC problem. So the light field display method [17]–[22] based on the MLA is considered as one of the most feasible approaches for 3D display, which supports the control of tightly clustered bundles of light rays and comfortable 3D scene by solving the AC problem.

Recently, researchers have proposed several methods to expand the DOF of near-eye light field display based on MLA. A tunable lens [23], [24] combined with other optical components as the relay optical element. The focal length of the relay optical element can be adjusted by applying different voltages to the liquid crystal lens. Therefore, the DOF of near-eye light field display system can be extended. However, these displays require time multiplex to provide images under a very high refresh rate to avoid the stroboscopic phenomenon, which is a challenge to the power dissipation and the drive of the device. In addition, integral imaging displays consisting of double or multilayered display devices [11], [25]–[27] have been reported. But those methods are inappropriate and impossible to implement in near-eye display system.

In this paper, a prototype of hybrid computational near-eye light field display based on MLAs is proposed, which is capable of rendering a reconstructed 3D scene with an extended DOF and nearly accurate focus cues. As our knowledge, the new algorithm for optimizing the structure parameters of hybrid computational near-eye light field display based on double MLAs is first proposed in this paper. Our primary technical contributions are:

- We propose a prototype of hybrid computational near-eye light field display based on MLA, which is capable of synthesizing sharp images of virtual and augmented reality objects within a correct accommodation range. Meanwhile, we evaluate the capability of MLA to create an extended hybrid DOF through optical analysis. And we also discuss the influence of the different gaps between micro-lens array (MLA) and element image plane (EIA).
- An algorithm for optimizing the structure parameters is also discussed by analyzing the spatial domain and frequencies domain of this system to lessen the system's ray resolution and the mismatching between the reconstructed light field L ' and the object's real light field L.

This paper is organized as follows. Section 2.1 describes the proposed prototype which includes the schematic of the proposed system and the analysis of DoF. In section 2.2, we focus on the structure parameters prioritization method (SPPM). Section 3 and Section 4 show the experimental results and conclusions, respectively.

2. Principle

In order to solve the narrow DoF problem in near-eye light field display based on MLA, a new construction with two MLAS and two beam splitters is proposed. This section describes how to expand the DoF of the virtual object. In addition, we will also introduce the structure parameters prioritization method (SPPM) based on analyzing the system's ray resolution and the spectra difference between reconstructed light field and the object's real light field.

2.1 Schematic of the Proposed System and DoF-Enhanced

Figure 1 presents a schematic of the proposed system. Through placing a beam splitter 1 in front of two integral-imaging systems (IIs) with different gaps between micro-lens array (MLA) and element image plane (EIA), the optical axis can be separated into two directions. Both rays coming from the real world and the IIs can enter human pupil through beam splitter 2.

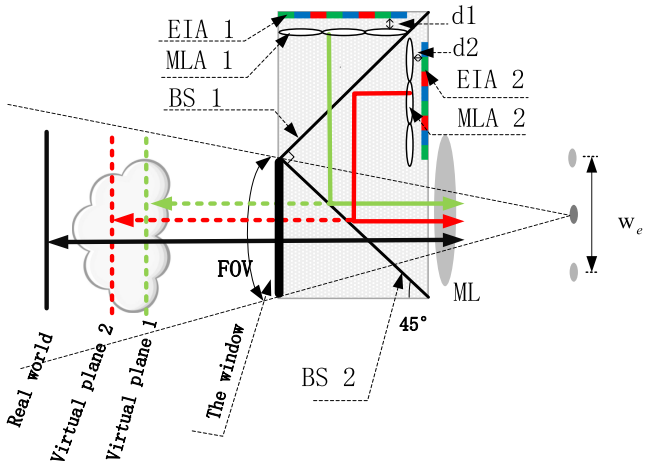

Fig. 1. Schematic of the configuration of the proposed system.

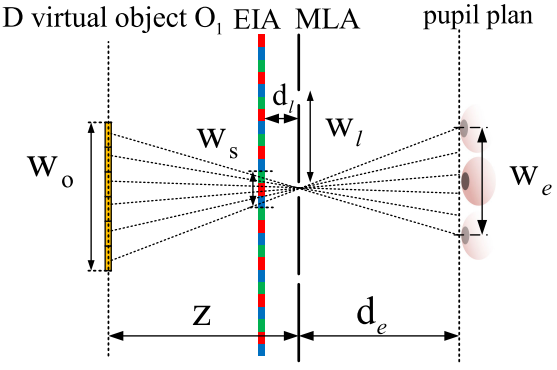

Fig. 2. The potential DoF of the conventional IIs.

As shown in Fig. 2, referring to the early report [11], [28], the potential DoF of the conventional IIs considers the facet braiding, which can be obtained as follow:

$$D_{DOF} = \frac{2z^2 p d_l w_l}{d_l^2 w_l^2 - p^2 z^2} \tag{1}$$

Where z is the distance between virtual object W_o and MLA, p denotes the pixel pitch of the display panel, the gap between EIA and MLA is d_l, and W_l is the pitch of MLA. It can be seen that, for a given display panel and MLA, the DOF is inversely proportional to d_l. There are three kinds of conditions considering two MLAs and Two EIAs in the reconstructed region as shown in Fig. 3:

- DOF1 and DOF2 overlap with each other, as shown in Fig. 4(a);
- DOF1 and DOF2 are separated, but connected, as shown in Fig. 4(b);
- DOF1 and DOF2 are completely separated with large distance.

Considering reconstructing the virtual object with a continuous DOF, here we just discuss the condition 1 and condition 2, where the two MLAs and ELAs have identical specifications, but the distance d_l between MLA and EIA are distinct. Non-zero $D_{ov} = z_1\text{-}z_2+(D_{MLA1}+ D_{MLA2})/2$ is the overlapped part for the condition 1. As discussed earlier, D_{tot_gen} can be obtained as follows:

$$D_{tot\_gen} = D_{MLA1} + D_{MLA2} - D_{ov} = \frac{z_1^2 p d_{l1} w_l}{d_{l1}^2 w_l^2 - p^2 z_1{}^2} + \frac{z_2^2 p d_{l2} w_l}{d_{l2}^2 w_l^2 - p^2 z_2^2} - z_1 + z_2 \tag{2}$$

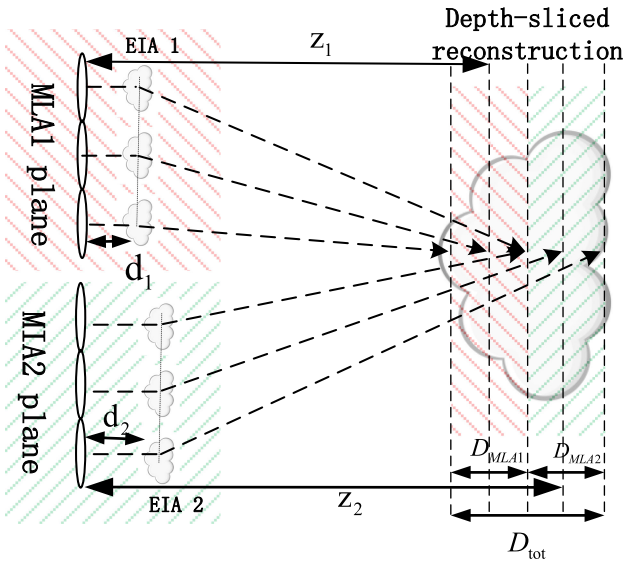

Fig. 3. Different focusing of bifocal IIs.

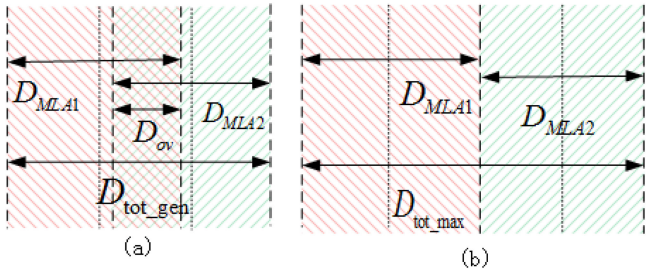

Fig. 4. (a) DOF1 and DOF2 overlap with each other. (b) DOF1 and DOF2 are separated, but they are connected.

Where non-zero D_{ov} is the overlapped part for the condition 1. If D_{ov} equal to zero, the D_{tot_max} for condition 2 can be obtained as follows:

$$D_{tot\_max} = D_{MLA1} + D_{MLA2} = \frac{2z_1^2 p d_{l1} w_l}{d_{l1}^2 w_l^2 - p^2 z_1^2} + \frac{2z_2^2 p d_{l2} w_l}{d_{l2}^2 w_l^2 - p^2 z_2^2} \tag{3}$$

Based on the above analysis, the extended depth range D_{tot_gen} or D_{tot_max} of the reconstructed light field with the new construction with two MALs and two beam splitters obviously bigger than DMLA1 or DMLA2 with only one MLA. So our new structure successfully enhance the DOF range of the reconstructed light field.

2.2 Structure Parameters Prioritization Method (SPPM)

The object's real light field L can be recorded by Light Field camera or camera arrays as multi-viewpoints images in a certain range of orientations. In other words, a set of multi-viewpoints images with fixed disparity values represent the real light field alone the record orientation. The DOF of the real light field L can be accurately obtained by counting these disparity values. Meanwhile, the DOF is related to the parameters of stereo display system, such as the pitch, the focal length of MLAs, and the number of pixels under one micro-lens. Aiming to the best system performance, the SPPM

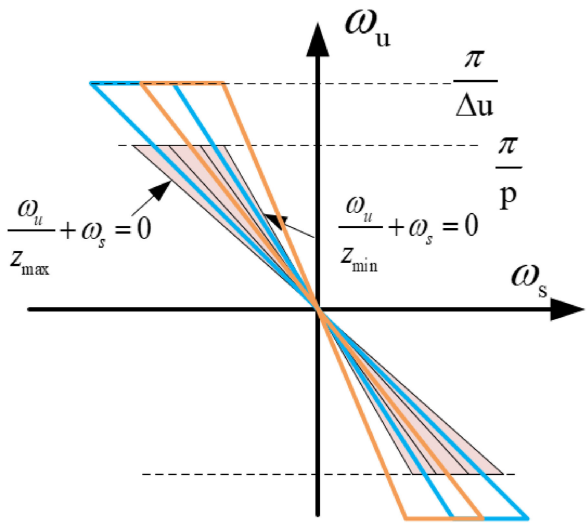

Fig. 5. The frequency domain of the original light field and reconstructed light field.

is proposed to optimize the structural parameters by analyzing the spatial domain and frequencies domain of this system.

Here the ray resolution η' is defined as the reciprocal of the number of rays which could enter into eye box passing though one pinhole from the reconstructed object. Theoretically, the lower value of ray resolution will result in higher angular resolution. As shown in Fig. 2, we assume an object W_0 locates at depth z, and a single MLA (or pinhole array) is placed at a distance d_l in front of an elemental image W_s and pixel size p. In addition, the viewer with eye box size W_e stand at the distance d_e to the MLA. The value of pixels located at W_s are determined by the rays from the objet W_0, and the size W_s can be calculated by $W_e{}^*d_l/d_e$. So the average number of light rays passing through one pinhole located at W_s is $W_e{}^*d_l/(p^*\ d_e)$. Since the pinhole with smaller ray resolution η' means that it can modulate more rays to reconstruct the virtual object W_0, the retina can receive the reconstructed light fields with higher angular resolution. Therefore, the ray resolution η' is an important parameter to evaluate the reconstructed precision of the system we proposed. It can be described by:

$$\eta' = \min\left(\frac{p^*d_e}{W_e{}^*d_{l1}}, \frac{p^*d_e}{W_e{}^*d_{l2}}\right) \tag{4}$$

The other important factor causing the reduction of reconstructed precision is the difference between reconstructed light field L' and the object's real light field L. As shown in Fig. 5, the depth range of the scene is $[Z_{min}, Z_{max}]$, and the maximum spatial resolution is $|\omega_s| \le \pi/p$. The slope of each line through the origin of the coordinate system is related to the depth of the virtual object. The range of the frequency domain of the original light field is from the farthest plane $\omega_u/z_{max} + \omega_s = 0$ to the nearest plane $\omega_u/z_{min} + \omega_s = 0$. According to the early report, the frequency domain of conventional computational light field $L_s(\omega_u, \omega_v, \omega_s, \omega_t)$ can be described as:

$$L_s(\omega_u, \omega_v, \omega_s, \omega_t) = \sum_{m_1,m_2,l_1,l_2\in Z} L'\left(\omega_u - \frac{2\pi m_1}{p}, \omega_v - \frac{2\pi m_2}{p}, \omega_s - \frac{2\pi l_1}{w}, \omega_t - \frac{2\pi l_2}{w}\right) \tag{5}$$

Where $m_1.m_2$, l_1, $l_2 \in z$ and z is a set of integers. The above equation indicates that $L_s(\omega_u, \omega_v, \omega_s, \omega_t)$ consists of replicas of the Fourier transform of reconstructed light field $L'_s(\omega_u, \omega_v, \omega_s, \omega_t)$. The 2D slice of the 4D Function can be obtained:

$$L_s(\omega_u, \omega_s) = \sum_{m_1,l_1\in Z} L'\left(\omega_u - \frac{2\pi m_1}{p}, \omega_s - \frac{2\pi l_1}{w}\right) \tag{6}$$

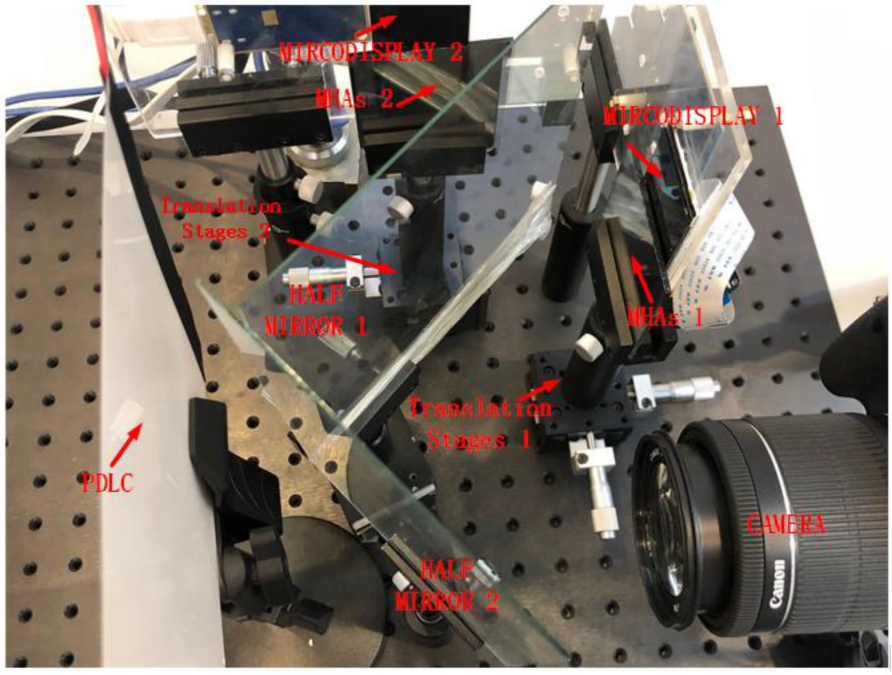

Fig. 6. Photographs of the prototype.

The shape of the frequency domain of $L_s(\omega_u, \omega_s)$ is shown as the blue closed region in Fig. 5. The farthest plane $\omega_u/z_{max} + \omega_s = 0$ of the original light field is lower than left border of the frequency domain of the blue region. In this case, we can only reconstruct a clear light field L' over the blue light field's farthest plane. Similarly, the nearest plane $\omega_u/z_{min} + \omega_s = 0$ of the original light field is higher than the bottom of the frequency domain of the yellow line, but lower than the top line. It means that the ability of light field reconstruction will be wasted. So the difference between L and L' will decrease the resolution of the reconstructed object.

The frequency domain of our proposed system is the sum of the blue and yellow region, and it is clear that we could get a larger range of the frequency domain of light field which can closely match the original 3D scene's frequency domain. According to the above analysis, we propose a new arithmetic of SPPM to minimize the overlapping rate and the difference between reconstructed light field L' and original light field L, which can be expressed as:

$$\arg\min_{d_{l1}, d_{l2} > \Delta d_l} (|\omega_{max}| + |\omega_{min}| + \eta'), d_{l1} z_{min\,2} \leq d_{l2} z_{min\,1} \tag{7}$$

Where $\omega_{max} = d_{l1}/z_{max\,1} - 1/z_{max}$ and $\omega_{min} = d_{l2}/z_{min\,2} - 1/z_{min}$ are the offset of the bottom and top boundary of the frequency domain of L and L', respectively. The depth range of two IIs are $[Z_{min1}, Z_{max1}]$ and $[Z_{min2}, Z_{max2}]$, respectively, which can be calculated by the Eq. (1). $\triangle d_l$ is the thickness of the glass substrate on the micro display. Therefore, whether the spatial frequency of the original light field is higher or lower, the spectra between the original light field and the reconstructed light field and ray resolution can be minimized.

3. Experimental Details

To demonstrate the feasibility of the proposed system, a new prototypes carried out shown in Fig. 6 and the parameters of this system are shown in TABLE 1.

In this experiment, the near-eye light field display consists of two Integral-imaging systems with Micro-hole pitch of 0.129 mm. The sub-pixel size and resolution of the LCD panel are 0.01075 mm

TABLE 1
The Structure Parameters of This System

Items	Unit	Value
The sub-pixel size of LCD Panel	mm	0.01075
The resolution of LCD Panel	-	1920×1080
Micro-hole pitch	mm	0.129
Gap	mm	1.1 and 1.4
Eye box	mm	6
Object plane	mm	1000

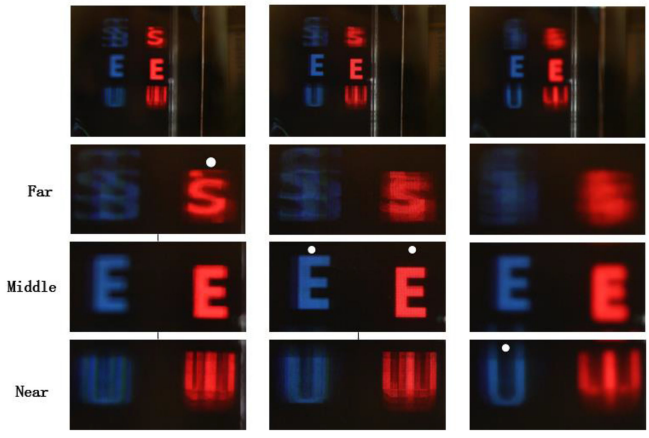

Fig. 7. The result of experiment 1: VR mode.

and 1920×1080, respectively. Due to the similar imaging principle between MLAs and micro-holes arrays (MHAs), MLAs are replaced by MHAs with higher accurate in our system. The gap dl between MHAs and the panel are adjusted to form a virtual image at a different distance. The retinal imagines of the reconstructed light field are taken by a camera (Canon EOS 700D) with the F-number of 5.6 and focal length of 22 mm corresponding to the pupil diameter of 4 mm.

There are two modes that the VR mode is shown in experiment 1 and the AR mode is shown in experiment 2, which can be switched by close or open the window (made by PDLC) in front of the second beam splitters. VR mode is shown in Fig. 7. The original light field of each IIs is composed of three letters from far to near, 'S', 'E' and 'U', respectively. Furthermore, the resolution of original light field L is 1920×1080, and the number of viewpoints is 4×4. The reconstructed light fields after being fused by two BS are taken by camera, as shown in Fig. 7. Due to the different gap d_l, there are two central depth plan (CDP) in the reconstructed region. With the prototype shown in Fig. 6, the perceived images at different depth are taken by the camera. Retinal blur is clearly observed from the results and the support of accommodation cues is confirmed with the enlarged DOF. In Fig. 7, the images at the top of each column are the perceived images with different depth. The enlarged parts of accommodation depths corresponding to the perceived images are listed below. Especially, the enlarged parts with a white spot show sharp images which indicate the matching between accommodation depths of the camera and the depth of reconstructed virtual object.

For AR mode, the display pattern is a part of resolution target image USAF 1951, as shown in Fig. 8. The panel 1 displays the pattern (a), (b) and (c) in different depth, and the pattern (d), (e) and (f) are rendered by the panel 2. The Fig. 8(b) shows the illustration of positions in the reconstructed region. Three real objects (Rubik's Cube, Pottery Figurine and Toy Car) are placed at the different

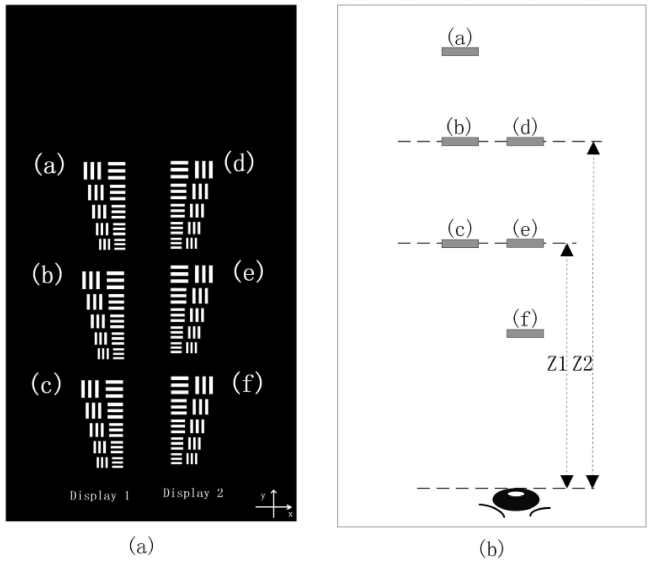

Fig. 8. The illustration of positions in the reconstructed region.

TABLE 2
The Different Parameters of the Gap Between MHAs and Micro-Display

	1	2	3	4	5	6	7
d_{l1} (mm)	0.95	1.05	1.45	1.85	2.25	2.65	3.05
d_{l2} (mm)	1.25	1.35	1.75	2.15	2.55	2.95	3.35

depth in the real world, and two rows of the pattern are the reconstructed virtual object rendered by two LCD panels, respectively. The comparison experiment results with continuous focus cues are listed in the left side, and the sharp perceived image of the pattern is obtained at the depths where the camera focuses at. Fig. 9 demonstrates the display results of see-through mode with our methods. It clearly shows that the upper left of pattern with larger diopter rendered by LCD1 panel is sharp when camera focus at the Rubik's Cube. In contrast, the upper right one rendered by LCD2 panel is bluer. The center row, both of them are sharp corresponding the depth plane of Pottery Figurine, but the right pattern is much more natural and sharp than the left one. The right pattern appears in focus, while the left one appear out of focus corresponding the depth plane of Toy Car.

According to the results, by adjusting the gap the MHAs and microdisplay, our prototype can reconstruct two light fields with a partially overlapped DOF, which proves the ability of accommodation of the reconstructed light field display. Meanwhile, compared to the limited accommodation distance of single DOF, such as the left pattern rendered by LCD1 panel, or the right pattern rendered by LCD1 panel, our prototype can provide an expanded DOF from the farthest Rubik's cube to the nearest Toy Car.

To demonstrate the optimal performance of structure parameters prioritization method (SPPM), we test the system with 7 group parameters with different gap d_l between MHAs and micro-display, as shown in TABLE 2. The distance is adjusted by translation stages, as shown in Fig. 6. Fig. 10 shows those in-focus perceived images of three letters in different depths. We can easily find that all of those perceived images are reconstructed with high contrast at the corresponding depths,

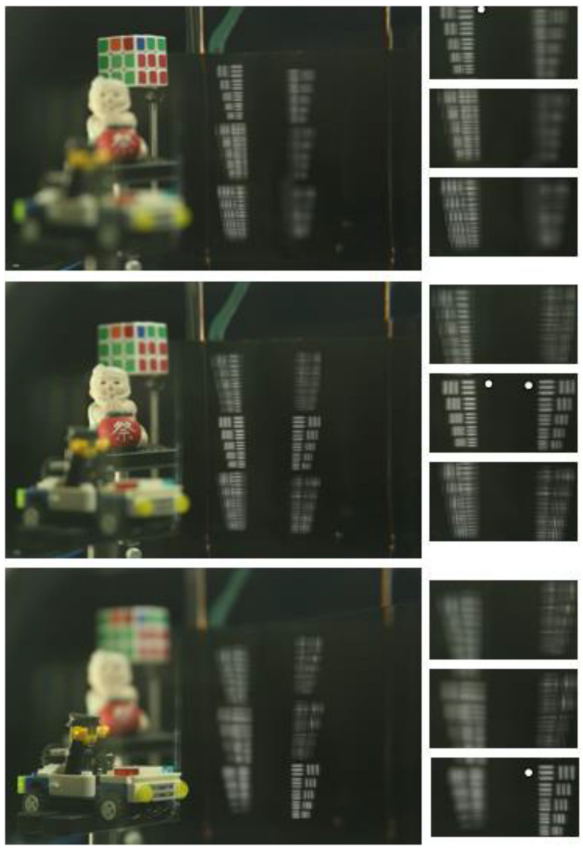

Fig. 9. The result of experiment 2: AR mode.

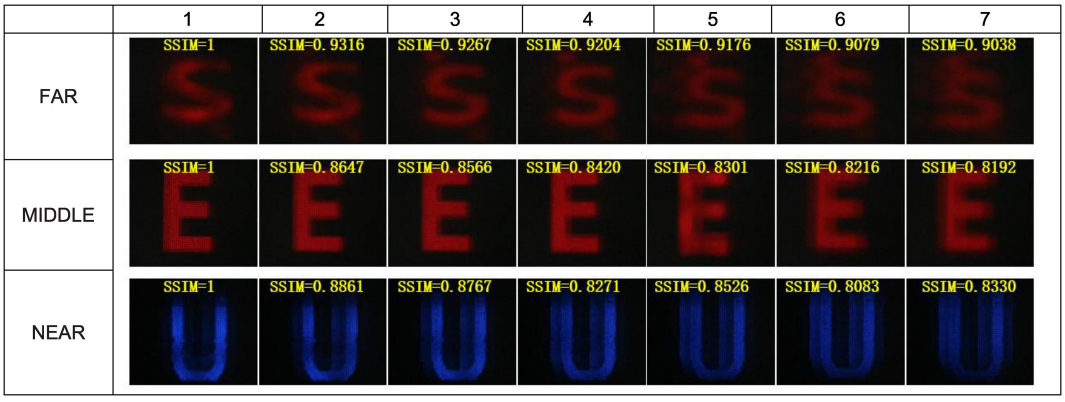

Fig. 10. The perceived images of the three letters with combined the well-focused depth slices utilizing 7 groups of structure parameters. Each row show the reconstructed light field of the letters corresponding to different gaps and each column shows the different depth.

and the perceived images in the first columns are distinguishable with sharp profile. So we test the structural similarity index (SSIM) of those perceived images compared with the first columns. Expansion gaps will lead to high levels of crosstalk which can make retinal images hard to focus and lack fidelity. However the SSIM date in Fig. 10 demonstrate that the margin error from the second to fifth group is limited to less than 4 percent, which verifies the optimized capability of our SPPM.

4. Conclusions

We proposed a novel hybrid near-eye light field display based on MLA to improve the DoF of the reconstructed light field, which is capable of expanding the accommodation range for virtual and augmented reality. The new algorithm for optimizing the structure parameters of hybrid computational near-eye light field display is proposed to lessen the ray resolution and the mismatching of the reconstructed light field. We evaluate the capability of extending DOF through optical experiment. It shows that the propose system can effectively expand the depth range in near-eye displays.

References

[1] H. Huang and H. Hua, "Systematic characterization and optimization of 3D light field displays," *Opt. Exp.*, vol. 25, no. 16, pp. 18508–18525, Aug. 7, 2017.
[2] H. Arimoto and B. Javidi, "Integral three-dimensional imaging with digital reconstruction," *Opt. Lett.*, vol. 26, no. 3, pp. 157–159, 2001.
[3] K. Akeley, S. J. Watt, A. R. Girshick, and M. S. Banks, "A stereo display prototype with multiple focal distances," *ACM Trans. Graph.*, vol. 23, no. 3, pp. 804–813, Aug. 2004.
[4] G. Favalora, "Volumetric 3D displays and application infrastructure," *Computer*, vol. 38, no. 8, pp. 37–44, 2005.
[5] S. Lee, C. Jang, S. Moon, J. Cho, and B. Lee, "Additive light field displays: Realization of augmented reality with holographic optical elements," *ACM Trans. Graph.*, vol. 35, no. 4, pp. 1–13, 2016.
[6] A. Maimone, A. Georgiou, and J. S. Kollin, "Holographic near-eye displays for virtual and augmented reality," *ACM Trans. Graph.*, vol. 36, no. 4, pp. 1–16, 2017.
[7] G. D. Love1, D. M. Hoffman, P. J. W. Hands, J. Gao, A. K. Kirby, and M. S. Banks, "High-speed switchable lens enables the development of a volumetric stereoscopic display," *Opt. Exp.*, vol. 17, no. 18, pp. 15716–15725, 2009.
[8] S. Lee *et al.*, "Foveated retinal optimization for see-through near-eye multi-layer displays," *IEEE Access*, vol. 6, pp. 2170–2180, 2018.
[9] K. J. MacKenzie, D. M. Hoffman, and S. J. Watt, "Accommodation to multiple-focal-plane displays: Implications for improving stereoscopic displays and for accommodation control," *J. Vis.*, vol. 10, no. 8, pp. 1–20, Jul. 1, 2010.
[10] S. Liu and H. Hua, "A systematic method for designing depth-fused multi-focal plane three-dimensional displays," *Opt. Exp.*, vol. 18, no. 11, pp. 11562–11573, May 24, 2010.
[11] Y. Kim, J.-H. Park, H. Choi, J. Kim, S.-W. Cho, and A. B. Lee, "Depth-enhanced three-dimensional integral imaging by use of multilayered display devices," *Appl. Opt.*, vol. 45, no. 18, pp. 4334–4343, 2006.
[12] M. Liu, C. Lu, H. Li, and X. Liu, "Bifocal computational near eye light field displays and structure parameters determination scheme for bifocal computational display," *Opt. Exp.*, vol. 26, no. 4, pp. 4060–4074, Feb. 19, 2018.
[13] J. Zhao and J. Xia, "Virtual viewpoints reconstruction via Fourier slice transformation," *J. Soc. Inf. Display*, vol. 26, no. 8, pp. 463–469, 2018.
[14] S. W. Min, B. Javidi, and B. Lee, "Enhanced three-dimensional integral imaging system by use of double display devices," *Appl. Opt.*, vol. 42, no. 20, pp. 4186–4195, Jul. 10, 2003.
[15] D. Lanman, M. Hirsch, Y. Kim, and R. Raskar, "Content-adaptive parallax barriers: Optimizing dual-layer 3D displays using low-rank light field factorization," *ACM Trans. Graph.*, vol. 29, 2010, Art. no. 163.
[16] D. Lanman, G. Wetzstein, M. Hirsch, W. Heidrich, and R. Raskar, "Polarization fields: Dynamic light field display using multi-layer LCDs," *ACM Trans. Graph.*, vol. 30, 2011, Art. no. 186.
[17] H. Hua and B. Javidi, "A 3D integral imaging optical see-through head-mounted display," *Opt. Exp.*, vol. 22, no. 11, pp. 13484–91, Jun. 02, 2014.
[18] F.-C. Huang, K. Chen, and G. Wetzstein, "The light field stereoscope: Immersive computer graphics via factored near-eye light field display with focus cues," *ACM Trans. Graph.*, vol. 34, no. 4, 2015, Art. no. 60.
[19] H. Huang and H. Hua, "An integral-imaging-based head-mounted light field display using a tunable lens and aperture array," *J. Soc. Inf. Display*, vol. 25, no. 3, pp. 200–207, 2017.
[20] M. Li, L. Wang, W. Shen, D. Wu, and Y. Bai, "Microlens array expander with an improved light intensity distribution throughperiodic submicro-scale filling for near-eye displays," *Appl. Opt.*, vol. 57, no. 5, pp. 1026–1036, Feb. 10, 2018.
[21] G. Wu *et al.*, "Light field image processing: An overview," *IEEE J. Sel. Topics Signal Process.*, vol. 11, no. 7, pp. 926–954, Oct. 2017.
[22] T. Zhan, Y. H. Lee, and S. T. Wu, "High-resolution additive light field near-eye display by switchable pancharatnam-berry phase lenses," *Opt. Exp.*, vol. 26, no. 4, pp. 4863–4872, Feb. 19, 2018.
[23] X. Shen and B. Javidi, "Large depth of focus dynamic micro integral imaging for optical see-through augmented reality display using a focus-tunable lens," *Appl. Opt.*, vol. 57, no. 7, pp. B184–B189, Mar. 1, 2018.
[24] X. Shen, Y. J. Wang, H. S. Chen, X. Xiao, Y. H. Lin, and B. Javidi, "Extended depth-of-focus 3D micro integral imaging display using a bifocal liquid crystal lens," *Opt. Lett.*, vol. 40, no. 4, pp. 538–41, Feb. 15, 2015.
[25] D.-Q. Pham *et al.*, "Depth enhancement of integral imaging by using polymer-dispersed liquid-crystal films and a dual-depth configuration," *Opt. Lett.*, vol. 35, no. 18, pp. 3135–3137, 2010.
[26] C. J. Kim, M. Chang, M. Lee, J. Kim, and Y. H. Won, "Depth plane adaptive integral imaging using a varifocal liquid lens array," *Appl. Opt.*, vol. 54, no. 10, pp. 2565–2571, Apr. 1, 2015.
[27] D. Kim, S. Lee, S. Moon, J. Cho, Y. Jo, and B. Lee, "Hybrid multi-layer displays providing accommodation cues," *Opt. Exp.*, vol. 26, no. 13, pp. 17170–17184, Jun. 25, 2018.
[28] S. Yang, X. Sang, X. Yu, X. Gao, and B. Yan, "Analysis of the depth of field for integral imaging with consideration of facet braiding," *Appl. Opt.*, vol. 57, no. 7, pp. 1534–1540, Mar. 1, 2018.